Using Successive Self-nucleation and Annealing (SSA) to detect the solid-solid transitions in poly (hexamethylene carbonate) and poly (octamethylene carbonate)

Ricardo Arpad Pérez-Camargo[1], Guoming Liu[1,2], Leire Meabe,[3] Ying Zhao[1,2], Haritz Sardon[3], Alejandro J. Müller[3,4*] and Dujin Wang[1,2]*

[1] CAS Key Laboratory of Engineering Plastics, Beijing National Laboratory for Molecular Sciences, Chinese Academy of Sciences, Beijing, 100190, China.

[2]University of Chinese Academy of Sciences, Beijing 100049, China

[3]POLYMAT and Department of Polymers and Advanced Materials: Physics, Chemistry and Technology, Faculty of Chemistry, University of the Basque Country UPV/EHU, Donostia-San Sebastián, 20018, Spain.

[4]IKESBASQUE, Basque Foundation for Science, Plaza Euskadi 5, Bilbao, 48009, Spain.

*Corresponding authors: Guoming Liu (gmliu@iccas.ac.cn) and Alejandro J. Müller (alejandrojesus.muller@ehu.es)

For TOC use only

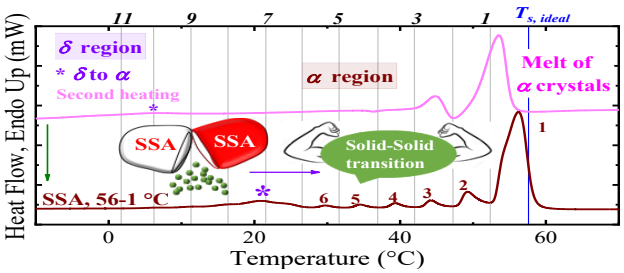

ABSTRACT

Solid-solid transitions in poly (hexamethylene carbonate) (PC6) and poly (octamethylene carbonate) (PC8), denoted δ to α transition, have been investigated, using self-nucleation and Successive Self-nucleation and Annealing (SSA) technique. The SSA protocol was performed *in-situ* for thermal (differential scanning calorimetry (DSC)), structural (Wide-angle X-ray Scattering (WAXS)), and conformational (Fourier-transformed Infrared Spectroscopy (FT-IR)) characterization. The final heating after SSA fractionation displayed an enhanced (compared to a standard second DSC heating scan) endothermic and unfractionated peak signal at low temperatures corresponding to the δ to α transition. The improved (i.e., higher enthalpy and temperature than in other crystallization conditions) δ to α transition signal is produced by annealing the thickest lamellae made up by α and β phase crystals after SSA treatment. As thicker lamellae are annealed, more significant changes are produced in the δ to α transition, demonstrating the transition dependence on crystal stability, thus, on the crystallization conditions. The ability of SSA to significantly enhance the observed solid-solid transitions makes it an ideal tool to detect and study this type of transitions. *In-situ* WAXS reveals that the δ to α transition corresponds to a change in the unit cell dimensions, evidenced by an increase in the *d*-spacing. This implies a more efficient chain packing in the crystal, for both samples, in the δ phase (lower *d*-spacing at low temperatures) than in the α phase (higher *d*-spacing at high temperatures). The chain packing differences are explained through *in-situ* FT-IR measurements that show the transition from ordered (δ phase) to disordered (α phase) methylene chain conformations.

Keywords: Self-Nucleation, Successive Self-nucleation and Annealing, Solid-solid transitions, crystal thickening-dependent behavior.

1. INTRODUCTION

Successive Self-nucleation and Annealing (SSA) is a well-established thermal fractionation technique that sequentially applies self-nucleation and annealing steps to a semicrystalline polymer. These sequential steps exploit the molecular segregation capacity exhibited by semicrystalline polymers.[1-3] Originally, the SSA technique was created as an alternative to other fractionation techniques, such as Temperature Rising Elution Fractionation (TREF), Crystallization Analysis Fractionation (CRYSTAF), and Step-Crystallization (SC).[1] Remarkably, SSA can fractionate a polymer in around 1 hour (in a conventional differential scanning calorimetry (DSC)[1-3]) or less (in a flash DSC[4,5]), without physical separation of the fractions, allowing the detection of intra and intermolecular defects.[1]

The SSA technique has been widely employed in polyolefins, in which quantitative analysis has been performed to determine: the ethylene sequence length distribution, the distributions of short-chain branching, stereo-defects, and lamellar thickness,[4,6] among others, as has been reviewed.[1-3] The SSA technique also brings important information, both qualitative and quantitative, in a wide range of homopolymers, and more complex systems, such as blends,[7] block copolymers,[8,9] and nanocomposites.[10] Recently, the SSA technique has been used in random copolymers,[11, 12] copolymers with different architectures,[13] and homopolymers with different chain topology (e.g., linear vs. cyclic).[14] These cases have revealed information related to the differences in chain topology and molecular architecture,[13,14] comonomer exclusion/inclusion balance,[11] the influence of nucleating agents,[10] and comonomer distribution caused by different comonomer addition protocols.[13] Recently, SSA has been employed to study the competition between crosslinking and chain extension in the postpolymerization of

polyamide 1012 (PA1012).[15] In view of all the wide range of applications of SSA, we decided to explore if it could be useful to study solid-solid transitions.

One of the most studied solid-solid transitions is the Brill transition in polyamides (PA). Structurally, the Brill transition is sharp since upon heating, the two main X-ray reflections merged into a single one with a *d*-spacing of 0.42 nm, at the Brill transition temperature, T_B. The transition is reversible, exhibiting hysteresis[16] since the T_B on heating is higher than on cooling. The Brill transition is considered a first-order transition that comprises a second-order element[17] since it is preceded by gradual crystallographic changes occurring over a relatively wide temperature range.[18] However, in the differential scanning calorimetry (DSC) traces, an endothermic peak for T_B is not usual for bulk crystallized samples, whereas a broad peak appears for crystallization from solution.[18] The Brill transition is highly dependent on the thermal history. It has been demonstrated that for isothermal crystallization from the melt, the higher the crystallization temperature, T_c, the higher the T_B.[18, 19] Similar changes in T_B are reported when solvents are employed.[20, 21] For PA1010 and PA1012, the T_B from single crystals[22] is higher when compared to that reported for bulk-crystallization.[23, 24] Yang et al.[25] determined that the T_B for PA1010 is a function of T_c and crystal size. They quenched and subsequently cold-crystallized the samples at different T_c, obtaining that as T_c increases, the T_B increases.[25] Recently, Wang et al.[26] study the effect of hydrogen bond organization by measuring the crystal perfection index (CPI) in PA1012. They found that the T_B values, after cooling at different rates (i.e., ranging from 5 to 100 °C/min) from the melt (i.e., 270 °C), decrease as CPI decreases (i.e., the low CPI are obtained at the highest cooling rates). But, if the PA1012 is molten at 210 °C, the distribution of hydrogen bonds is different, resulting in an independent CPI on the cooling conditions, revealing the importance of the hydrogen bond organization. In general, the position

of T_B is related to crystal perfection and crystal size. As the more perfect and bigger the crystals are, the T_B will be found in a higher position. However, recently, it has been pointed out that the amorphous phase may also play a key role,[17] as well as the hydrogen bond organization.[26]

The Brill transition has been widely studied in the polyamide family,[16,17, 26-28] and recently, a Brill-like transition has been reported for poly (octamethylene carbonate) (PC8)[29] and poly (hexamethylene dithiocarbonate) (PC6-D).[30] In PC8, Zhao et al.[29] reported the convergence, upon heating, of the d_{110} = 0.43 nm and d_{200} = 0.38 nm, observed at low temperatures (in the denoted α phase), into a single *d*-spacing at 0.41 nm at ~ 42 °C (in the denoted β phase). The β to α transition also occurs during cooling (reversible character), displaying a hysteresis effect. The α to β, and β to α transitions, were reflected on exothermic (β to α) and endothermic (α to β) peaks in the DSC traces after isothermally crystallizing the samples at 50 °C. The Brill-like transition was attributed to the reversible transition from *trans*-dominated conformations (in the α-phase (at low temperatures)) to the coexistence of *trans/gauche* conformations (in the β-phase (at high temperature)) of methylene sequences. Additionally, a weakening of the dipole-dipole interaction of the carbonyl groups was also observed.[29] These results were recently corroborated in PC8 by Pérez-Camargo et al.[31] Similar, but even clearer changes were found in PC6-D at higher temperatures due to the dithiocarbonate groups.[30] In both PC8 and PC6-D, an endothermic signal was clearly detected by using designed thermal protocols for amplification of the signals.[29,30] This demonstrated that solid-solid transitions signals could be enhanced with well-designed thermal protocols.

In a preceding work, it was shown that poly (hexamethylene carbonate) (PC6) and PC8 exhibited, during a non-isothermal test, solid-solid transitions at low temperatures[32] (resembling the above-described Brill-transitions[16,17,27]). Afterward, we demonstrated through isothermal

tests followed by non-isothermal scans, the presence of the denoted α to δ (during cooling) and δ to α (during heating) transitions, at low temperatures, in both PC6 and PC8, besides the Brill-like transition in the PC8.[31] The polymorphism on the PC8 includes the reversible δ to α and α to β transitions. The δ to α transition was attributed to the reversible change (at low temperature, e.g., below RT) between ordered to disordered conformations. Structurally the δ phase exhibited a more efficient package than the α phase.[31]

In this work, we investigate the use of the self-nucleation and the SSA technique to study the solid-solid transition in aliphatic polycarbonates, and how the thermal history affects the position of the δ to α, and α to β transitions. Considering the magnification of the changes generated under the SSA protocol, we have used it *in-situ* and simultaneously conducted a structural and conformational analysis with Wide-angle X-ray Scattering (WAXS) and Fourier-Transformed Infrared (FT-IR) spectroscopy, respectively. The SSA protocol demonstrated to be a useful technique in the study of the solid-solid transitions.

2. EXPERIMENTAL PART

2.1. Materials

Conventional polycondensation of aliphatic diols and dimethyl carbonate were used to prepare poly (hexamethylene carbonate) (PC6) and poly (octamethylene carbonate) (PC8) with number average molecular weight, M_n = 25100 and 15300 g/mol, respectively.[33] The previously established protocol in references 33,34 was followed. It consisted of a melt-polycondensation using 4-dimethylaminopyridine (DMAP) organocatalyst in two steps at 130 and 180 °C under vacuum. More details can be found in references 33 and 34.

2.2. Differential Scanning Calorimetry (DSC): Non-isothermal tests

The DSC experiments were conducted in a DSC model 8500 of Perkin Elmer. It was connected to controlled liquid nitrogen (N_2) cooling device, model CLN2, and operated with a constant flow of ultrapure N_2. The equipment was calibrated with indium and zinc standards at a rate of 20 °C/min. The samples as received, of *circa* 5 mg were encapsulated into aluminum DSC pans, and they were heated from room temperature (RT) to *T* (i.e., temperature to erase the thermal history: 85 °C (PC6) and 90 °C (PC8)), registering the first heating scan. They were held at *T* for 3 minutes to erase the thermal history. Afterward, a cooling scan from *T* to – 40 °C was performed, and a holding step at – 40 °C for 1 minute was used, stabilizing the sample. Subsequently, heating to *T* was performed, registering the second heating scan. More advanced protocols were employed, and the details are shown below.

2.3. DSC: Self-Nucleation (SN)

The SN experiments were performed according to the protocol established by Fillon et al.[35] The steps involved are represented schematically in Scheme 1.

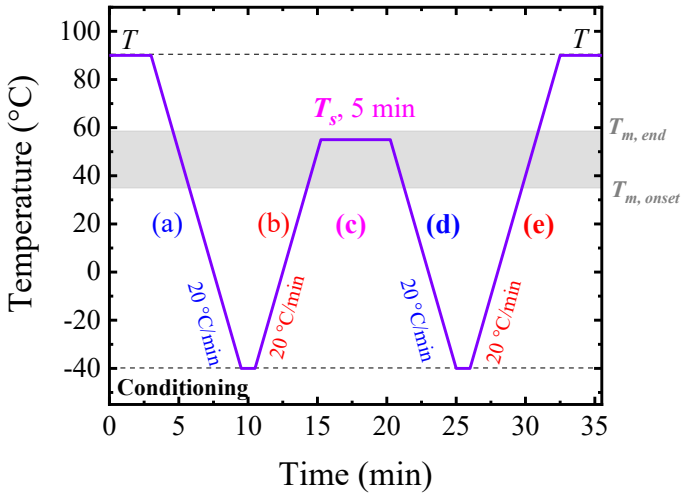

Scheme 1. Illustration of the SN steps, taking as an example the PC8. The shadowed region represents the melting range ($T_{m,\ onset}$ to $T_{m,\ end}$) of the PC8.

The first step of the SN protocol applied is (a) the conditioning step, in which a standard thermal history is created. In this case, the standard thermal history was created by cooling from the melt (temperature T, in Scheme 1, at which the thermal history is erased) to – 40 °C at 20 °C/min. Then, the sample is (b) heated to a selected SN temperature, T_s. The range of selected T_s values will cover the melting endotherm of the material, e.g., $T_{m,\ onset}$ to $T_{m,\ end}$, or higher ($T_s > T_{m,\ end}$) depending on the width of the SN domains. The definitions of the SN domains can be reviewed in references 1, 35-39. A brief explanation is presented below. After selecting a T_s, (c) the sample will be held at that temperature for 5 minutes. Then, the sample will be (d) cooled to – 40 °C at 20 °C/min and (e) subsequently heated to T at the same rate. By comparing the cooling (step d) and heating (step e) curves after step (c), the SN domains can be defined. Briefly, in *Domain I* or *the melting domain*, the cooling and heating curves resemble the standard curve, since the T_s cannot self-nucleate the sample. In *Domain II* or *SN Domain*, in (c), self-nuclei are created, and hence, in the subsequent cooling, the crystallization is enhanced, and the T_c is shifted to higher values due to a self-nucleation effect. This *SN Domain* does not generate changes in the melting behavior; therefore, the heating curves obtained in (e) resemble the standard heating. *Domain II* can be divided into *sub-Domains*: *Domain IIa* and *Domain IIb* based on the self-nuclei origin.[36-38] In *Domain IIa (melt memory region),* the T_s (in the higher temperature range of *Domain II,* i.e., $T_s > T_{m,\ end}$) is high enough to melt all the polymer crystals completely but without erasing its melt memory. Thus, non-crystalline structures (such as regions with residual local orientation) act as self-nuclei.[40] In *Domain IIb (self-seeding region),*

the T_s (in the lower temperature range of *Domain II*, i.e., $T_s < T_{m,\,end}$) melts the polymer crystals, but some crystal fragments survive and act as self-seeds.[38,39]

Finally, in *Domain III*, or *self-nucleation and annealing domain*, the material is partially melted. Hence, in (c), the unmolten crystals are thickened or annealed during the 5 minutes at T_s. Thus, a shift in the T_c is produced. In (e) the subsequent heating, there is an extra melting peak corresponding to the melting of the annealed crystals. From the described *Domains* in this work, we are interested in *Domain II* since the maximum shift in T_c without annealing, corresponds to the $T_{s,\,ideal}$. This temperature is used as a starting point for the Successive Self-nucleation and Annealing (SSA) experiments.[1] In this work we found $T_{s,\,idealPC6}$ = 56 °C and $T_{s,\,idealPC8}$ = 58 °C.

2.4. DSC: Successive Self-Nucleation and Annealing (SSA)

The SSA experiments were performed according to the protocol created and recently reviewed by Müller et al.[1-3,5] The different steps are represented schematically in Scheme 2.

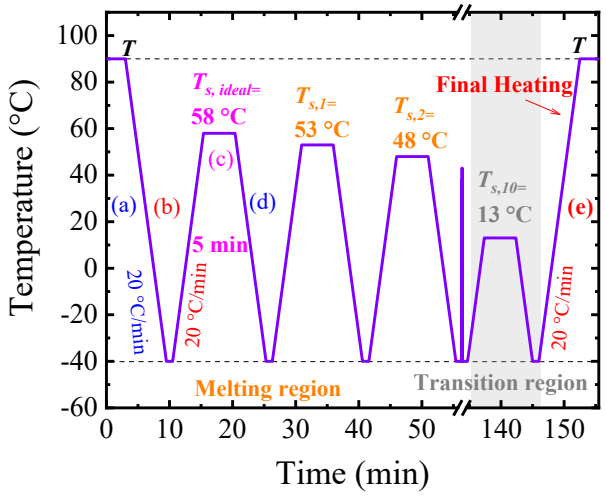

Scheme 2. Illustration of the SSA steps, taking as an example the PC8. The shadowed region represents the transition region of the PC8.

For the SSA test, we repeated the steps (a) to (d) of the SN, but in (c), the first T_s will be the $T_{s,\,ideal}$ of the selected material, e.g., 58 °C. Then, instead of heating until melting the material, as in (e) of the SN protocol, we heated the material until a $T_{s1}=T_{s,\,ideal}-5$ °C (e.g., 53 °C), since we use a fractionation window (FW) of 5 °C. The steps (a) to (d) were repeated at different T_s values (i.e., $T_s < T_{s,\,ideal}$) in (c), e.g., $T_{s,2}=T_{s,1}-5$ °C (e.g., 48 °C) in Scheme 2, generally to cover all the melting range of the material. After covering all the melting ranges of the material, we continued decreasing the T_s to cover the transition region (see shadowed region on Scheme 2), as well, reaching T_s values as low as 13 °C (see $T_{s,10}$ in Scheme 2). Once the fractionation of the material was achieved, the final SSA heating scan (see step (e) in Scheme 2) is performed, evidencing the different fractions resulting from the different steps at T_s. In this work, the $T_{s,\,ideal}$ of each material was used as starting point.

The selected parameters to perform the SSA experiments, were: scanning rate of 20 °C/min, FW of 5 °C, and holding times (i.e., fractionation time at each step) at T_s of 5 minutes. The SSA was performed in the range 56 to 1 °C and 58 to 13 °C for PC6 and PC8 respectively. To further understand the solid-solid transition, we also change the SSA parameters using different starting T_s, different ranges of temperatures, and FW of 5 and 10 °C. More details can be found in Section S1 of the SI.

2.5. *In-situ* SSA/WAXS experiments

The structural characterization was carried out in the Beijing Synchrotron Radiation Facilities (BSRF) at the beamline 1W2A. The SSA protocol was performed *in-situ*, placing the sample in a Linkam TST350 hot stage and taking WAXS simultaneously. For the WAXS experiments, we used a Pilatus 1M detector (resolution 981 x 1043 pixels), pixel size 172x172

μm^2, a wavelength of 1.54 Å, and a sample-to-detector distance of 140.9 mm. An exposure time of 10 seconds were employed.

2.6. *In-situ* SSA/FT-IR experiments

In-situ SSA experiments were conducted in the PC6 and PC8 samples, and simultaneously Fourier transform infrared (FT-IR) spectra were taken. Both PC6 and PC8 samples were previously film-cast in chloroform (5 mg of sample dissolved in 1 mL of chloroform) onto potassium bromide plates. Afterward, the samples were placed in a Linkam FTIR 600 hot stage coupled to a liquid nitrogen supply. A FT-IR spectrometer of Thermo Fisher model Nicolet 6700 was employed, recording FT-IR spectrum with a resolution of 4.0 cm^{-1} and coaddition of 32 scans per spectrum. The spectrum was recorded during the holding times of 1 minute at each selected temperature (i.e., holding steps at – 40 °C and T_s, and selected temperatures during the SSA final heating).

3. RESULTS AND DISCUSSIONS

3.1. Self-nucleation (SN)

SN experiments were conducted in the PC6 and PC8 samples in a preceding work,[32] determining that the carbonate groups influence the memory effect of the samples. The memory effect is caused by the self-nuclei, which remains when the SN at T_s produces a nonisotropic melt (i.e., *Domain IIa*).[38, 41] This effect is reflected in an increase of the crystallization temperature, T_c, and an unchanged melting temperature, T_m, during the DSC cooling and heating traces.[38, 41] In the specific case of aliphatic polycarbonates, in our previous work, it was found that the memory effect is present in the even-odd region (chain length, n_{CH2} = 6 to 9), and decreases as the n_{CH2} increases (due to the decreasing influence of the carbonate groups), until reaching its dilution in the saturation region (n_{CH2} = 10 to 12),[32] in line with the findings of Sangroniz et al.[41]

In this work, the SN experiments are focus on the evolution of solid-solid transition at low temperatures (below RT), denoted as δ to α, with T_s, and in the $T_{s,\ ideal}$ determination. Figure 1 shows the cooling and heating scans after the holding steps at the indicated T_s.

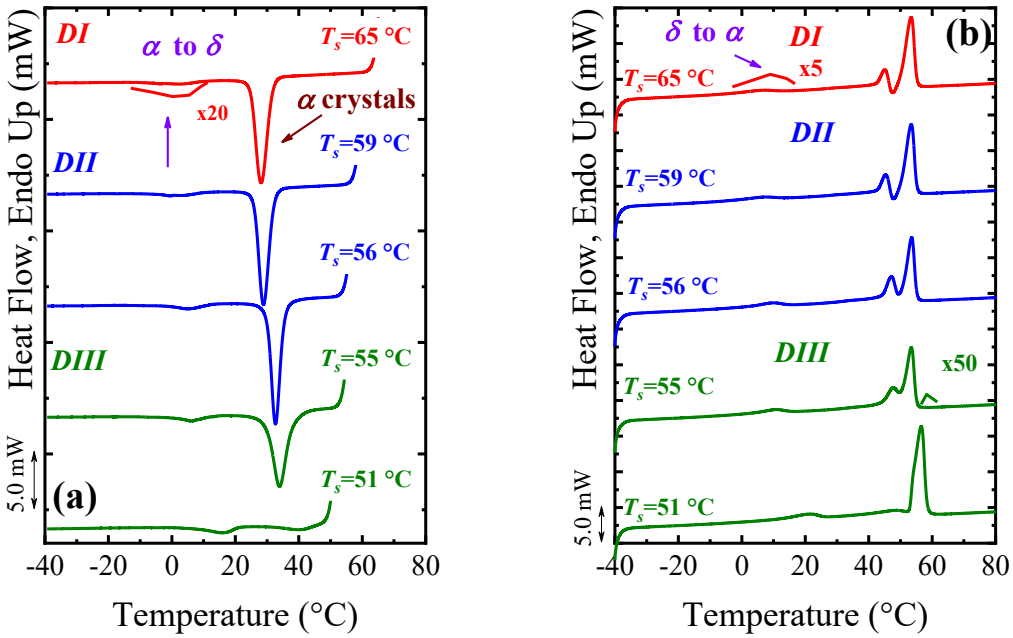

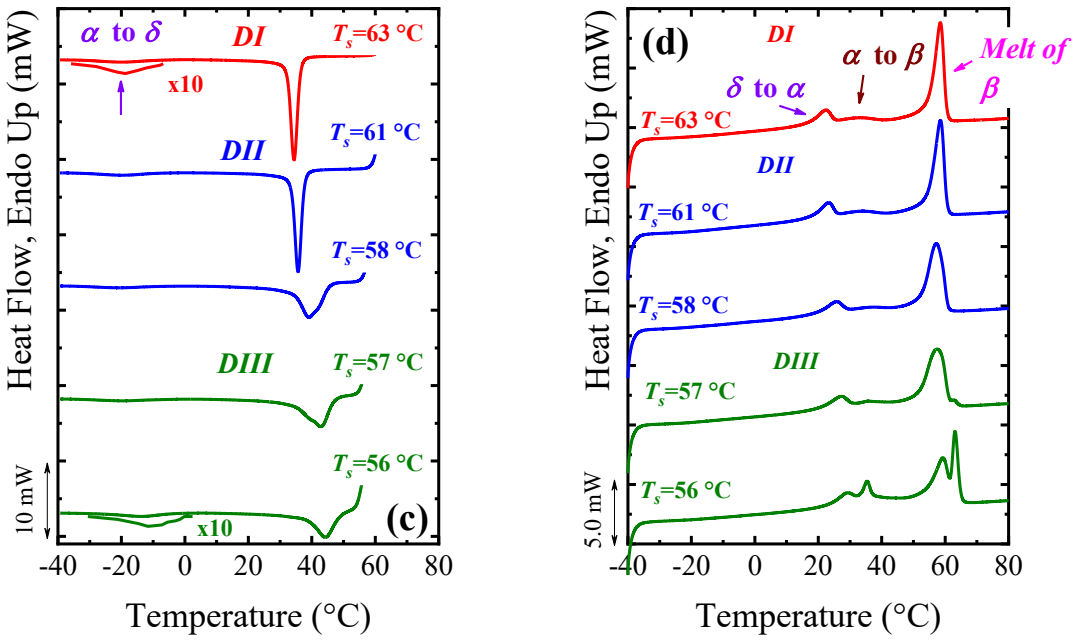

Figure 1. DSC (a) and (c) cooling scans after 5 minutes at the indicated T_s, and (b) and (d) subsequent heating scans after the cooling in (a) and (c) for PC6 (a and b), and PC8 (c and d). In all cases the scanning rate was 20 °C/min. Note that a color code was used for the different SN domains. Red color for *Domain I*, blue color for *Domain II*, and green color for *Domain III*. The solid-solid transition positions are indicated in the plot. Amplification of some signals is use for clarity.

In Figure 1, the resulting curves in *Domain I* are used to illustrate the 'standard' non-isothermal behavior since they are equivalent to the cooling and second heating scans of non-isothermal experiments (see Figure S1). These curves show the solid-solid transitions. During cooling, the denoted α to δ transitions are observed as a small exothermic peak at ~ 3 °C (PC6) and ~ – 20 °C (PC8) respectively. The large exothermic peaks in the cooling curves correspond to the crystallization process of the α (PC6) or β phase (PC8) at ~ 28 °C (PC6) and ~ 34 °C (PC8) respectively. In the subsequent heating, the reversibility of these transitions is observed at higher temperatures due to the hysteresis effect.[16] The δ to α transition, upon heating, occurs at ~ 6 °C

(PC6) and ~ 22 °C (PC8) respectively. In the case of PC6, the α crystals melt at ~ 53 °C, exhibiting a double melting peak, attributed to a complex reorganization process,[42] which was corroborated, in a preceding work,[32] by cooling at different rates. This reorganization process is also reflected in Figure 1b in the evolution from two (*Domains I* and *II*) to one (*Domain III*) endothermic peaks as T_s decreases. For PC8, there is an α to β (Brill-like transition as reported in the literature[29]) transition at ~ 33 °C, followed by the melting of the β crystals at ~ 58 °C. These transitions are in line with those reported by Zhao et al.[29] in PC8 and by us in a preceding work.[31]

Figure 1 shows the three SN domains for both PC6 and PC8. Additionally, we have found that PC6 exhibited *Domain IIa*, whereas PC8 only *Domain IIb* (see Figure S2). This behavior is explained by the weakening of the carbonyl groups influence as n_{CH2} increases.[32, 41] The SN limits are plotted in Figure S2 on the SI. From the *Domain II* to *III* transition, we determined the $T_{s,\ ideal}$ = 56 °C and 58 °C for PC6 and PC8, respectively.

In addition to the SN domains, Figure 1 also shows the different solid-solid transitions, at low temperatures, under the different SN domains. *Domain I* was discussed above. For PC6, in Domain *II*, due to the self-nucleation, the T_c is shifted to higher temperatures, from a value of 27.9 ºC up to 32.7 °C (Figure 1a at T_s = 56 °C), whereas the α to δ transition remains unchanged. Only in *Domain III* a shift to higher temperatures, from 3 to 16 °C at T_s = 51 °C, of the α to δ transition is observable.

Figure 1b exhibits the subsequent heating scans; as expected, both endothermic peaks (i.e., δ to α transition and melting of α crystals, T_m) remain at the same position in *Domain I* and *II*. In *Domain III* an extra high-temperature peak is observed due to the annealing of the α crystals at T_s = 55 °C. As in the cooling curves, the δ to α transition is shifted to higher temperatures, from 6

ºC to ~ 21 °C at T_s = 51 °C. Interestingly, such a shift to higher temperatures in the δ to α transition is produced by a T_s ~ 45 °C higher than the original temperature of the transition (during the second heating scan).

A similar behavior is observed for PC8 in Figures 1c and d. As in PC6, the solid-solid transitions remain unchanged in *Domain I* and *II,* and they are shifted to higher temperatures in *Domain III*. Interestingly, in *Domain III*, for T_s = 56 °C to 53 °C (see Figure 1d and S3) as the β crystals are annealed, increasing their melting signal, the endothermic signal of δ to α transition (~ 36 °C (PC8) lower than the selected T_s = 56 °C) became larger. Thus, the δ to α transition signal enhancement seems proportional to the crystal stability (i.e., lamellar thickness) at the annealing steps. The α to β transition is also shifted to higher temperatures and maintains a similar area. This might be related to its nature (i.e., an intermediate transition between the δ and β phases), and the narrow range of T_s that influence it. The evolution of the different peak positions as a function of selected T_s values can be clearly observed in Figure S4 on the SI. The SSA test reveals further information on the solid-solid transitions, as we show below.

In summary, the solid-solid transitions are not affected by self-nucleation in *Domains I* and *II*. These results could be expected because there is no crystal stability change (i.e., no annealing or lamellar thickening) in these two *Domains*. However, as annealing processes are present in *Domain III*, as the unmolten lamellar crystals at T_s tend to thicken during the 5 min holding time, the solid-solid transitions are also affected, as these transitions are related to different degrees of crystal stability (i.e., lamellar thickness).

3.2. Successive Self-nucleation and annealing (SSA)

The SSA experiments combine non-isothermal and isothermal steps, representing different crystallization conditions than those generally used in standard non-isothermal or isothermal

DSC experiments. This work investigates how such a combination of steps enhances the solid-solid transition signal, representing a helpful tool for their detection. As a starting point, we have used the $T_{s,\ ideal}$ for each sample: $T_{s,\ ideal}$ = 56 °C (PC6), and $T_{s,\ ideal}$ = 58 °C (PC8). Figure 2 shows the SSA final heating for PC6 (Figure 2a) and PC8 (Figure 2b) and their comparison with the second heating curve obtained through standard non-isothermal experiments.

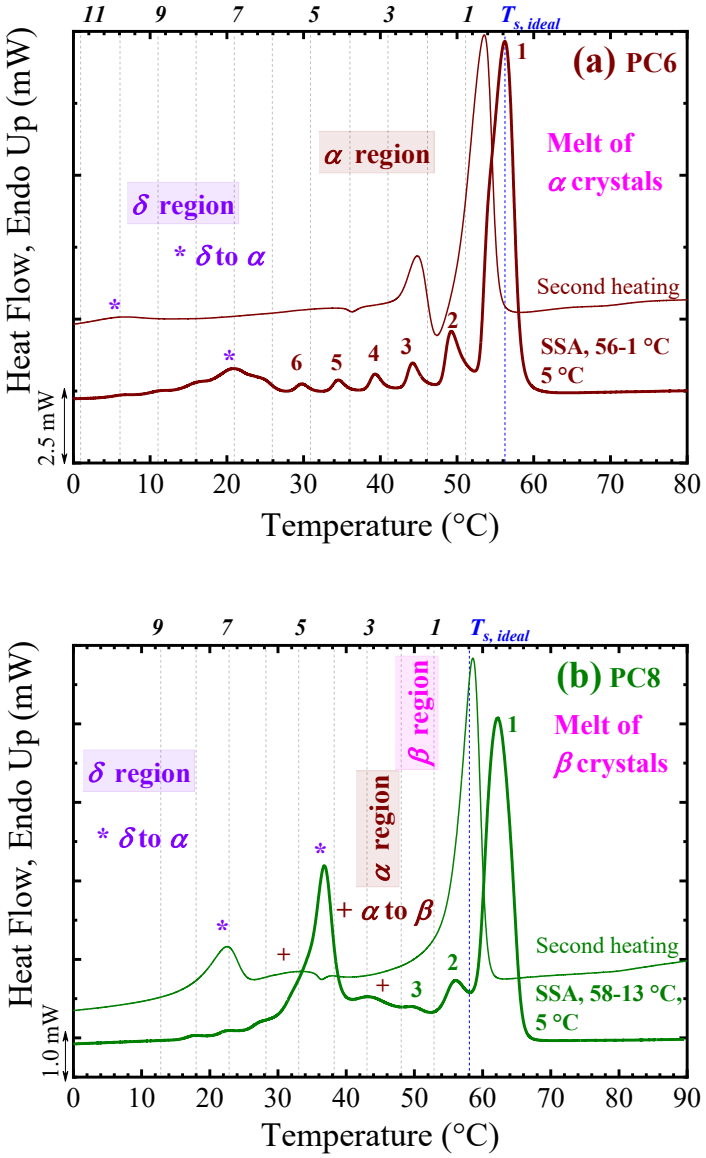

Figure 2. Final SSA heating DSC scans for (a) PC6 and (b) PC8. The asterisk (*) indicates the solid-solid transitions. The thinner lines represent the standard DSC second heating scans for

each sample. The vertical lines indicate the T_s used, and the numbers at the top represent the number of applied T_s values.

Figure 2 shows that both PC6 and PC8 can be thermally fractionated by SSA. Such fractionation in linear polymers is attributed to molecular weight distribution differences.[1] Interesting, the two prominent peaks and mostly unfractionated, indicated with an asterisk, at ~ 20 °C (PC6) and ~ 35 °C (PC8), are related to solid-solid transitions, denoted as δ to α transition. These peaks are shifted to higher temperatures (~ 14 °C for both PC6 and PC8) and exhibit more significant enthalpies (~ two (PC6) and three (PC8) times larger than in the standard second heating scan) than in the second heating scans, see Figure 2. It is worth noting that compared to our preceding work,[31] in which isothermal conditions were used, the δ to α transition is ~ 4 °C higher (for both PC6 and PC8), evidencing the influence of the crystallization conditions. Thus, the SSA technique improves the signal strength of the δ to α transition, helping its detection. As far as the authors are aware, this is the first time that SSA experiments are used to detect a solid-solid transition, achieving significant increases of the related signals.

Unfractionated peaks

The SSA protocol generates fractions of different lamellar thicknesses. Hence, after the SSA protocol, the final heating produces a distribution of melting points that reflects the distribution of lamellar thickness present in the sample after thermal fractionation.

Considering PC6 in Figure 2a, the $T_{s,\,ideal}$ = 56 °C does not generates any fraction, whereas T_{s1} = 51 °C produces fraction 1, T_{s2} = 46 °C produces fraction 2, and so on. For PC6, six fractions are generated by the SSA protocol, in which fraction number 6 is produced by T_{s6} = 26 °C. These fractions correspond to the α phase fractionation. At low temperatures (e.g., 5 to

25 °C), an unfractionated or poorly fractionated (by T_s < 26 °C) peak with a significant area (more extensive than the exhibited during non-isothermal DSC experiments) is observed. If a family of thin crystals generates this peak at low temperatures, it must be fractionated. However, the fraction's poor definition and the extensive area of the peak ~ 20 °C, evidence that it corresponds to the δ to α transition instead of a melting process. An analysis of the partial area of each fraction *versus* T_s also reflects two prominent peaks, corresponding to the δ to α transition and the melting process of the α or β phase (see Figures S5b and d). We also plotted the melting temperature of each fraction, in Figure 2, versus T_s, obtaining a linear relationship (see Figures S5a and c), which corroborated the correct application of the SSA fractionation protocol. It is worth noting that the large area of the signal and its position (i.e., higher temperatures than the second heating scan) indicates that increased crystal stability of the α (PC6) or β phase (PC8) also enhances the δ to α transition.

The above analysis can be extrapolated to PC8, see Figure 2b. In this case, two solid-solid transitions (i.e., δ to α and α to β) are present. The fractionation is only possible for a narrow range of high temperatures. Only three fractions are generated by T_s = 53 to 43 °C, corresponding to the β phase. In contrast, at lower temperatures, neither the α (i.e., below 55 °C), nor the δ (i.e., ~ 35 °C) phases, can be fractionated by T_s = 38 to 13 °C, as expected for solid-solid transitions.

Influence of the SSA conditions on the solid-solid transition

We have demonstrated that the δ to α transition signal after SSA shows a higher area and remains unfractionated. Such behavior is attributed to the annealing process, which simultaneously affects the most stable crystals and the solid-solid transition. This is observable for the δ to α transition in PC6 and PC8. To further understand how crystal stability affects the δ

to α transition, we have performed an SSA test with fractionation windows (FW) of 10 °C; hence, the $T_{s,1} = T_{s,\,ideal} - 10$ °C will anneal on average thinner crystals than using a FW of 5 °C. Figure 3 shows a comparison between the SSA final heating with FW of 5 and 10 °C, starting on the $T_{s,\,ideal}$ of each material.

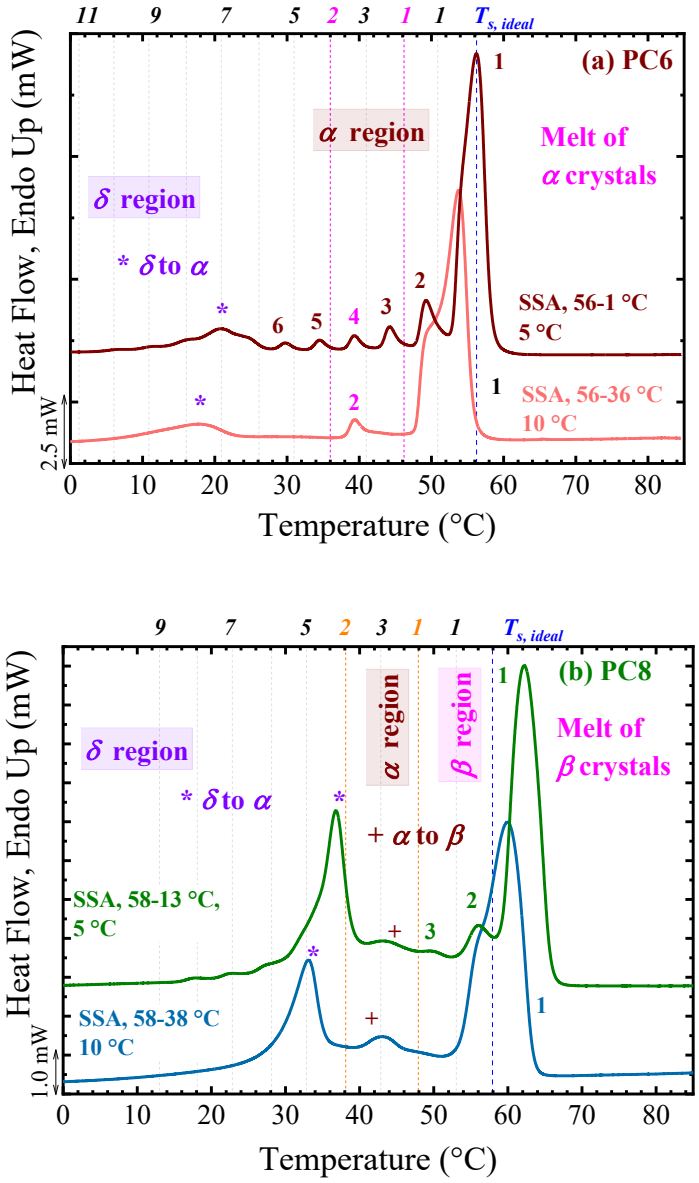

Figure 3. Comparison of the SSA final heating scans, using fractionation windows (FW) of 5 and 10 °C for (a) PC6, and (b) PC8. The colored numbers (at the top of the Figures) and vertical lines indicate the T_s used for the FW of 10 °C, while the rest of the numbers and vertical lines indicate the T_s for the FW of 5 °C.

Figure 3 show that the δ to α transition for FW of 10 °C is shifted to lower temperatures and possesses a lower area compared to that observed when a FW of 5 °C is used. The highest melting peaks (i.e., fraction 1, generated by $T_{s,1}$) are also at lower temperatures (for FW of 10 °C), as expected, indicating the higher crystal stability (i.e., thicker average lamellar crystals) reached when a FW of 5 °C is employed. The different position on the fractions and transition peaks is related to the crystal stability. The FW of 5 °C can anneal more crystals with a larger lamellar thickness (i.e., those annealed at the highest T_s), causing more significant changes in the position and area of the δ to α transition. In contrast, the FW of 10 °C, involves lower T_s (e.g., T_{s1} (FW of 10) will equal to T_{s2} (FW of 5)) which produces lower changes, as we prove by using different parameters in the SSA protocol (see Figures S6 to S7), and as we show below in Figure 4. Therefore, the improvement of the δ to α transition signal is proportional to the annealing of thicker crystals.

Besides the FW, we have evaluated the effect of the starting T_s (Figure S6) and the number of fractionation steps (Figure S7) on the δ to α transition. It has been found that the changes in the δ to α transition are mainly enhanced by the variation of FW while the starting T_s (see Figure S6) has a minor effect. Such behavior proves that the annealing of the thicker crystals generates most of the changes in the δ to α transition. Interestingly, the α to β transition (in PC8) does not show such an improvement, since the α phase is only affected (without influence the δ phase) in a narrow range of T_s values.

To illustrate that the annealing of larger crystals is the most important factor in affecting the δ to α phase, we have performed single SN experiments at different T_s values, including those used in the SSA experiments. Figure 4 shows the evolution of the endothermic peak of the δ to α

transition, $T_{\delta-\alpha}$, and the highest melting temperature value, T_{m1}, as a function of T_s for PC6 (Figure 4a) and PC8 (Figure 4b).

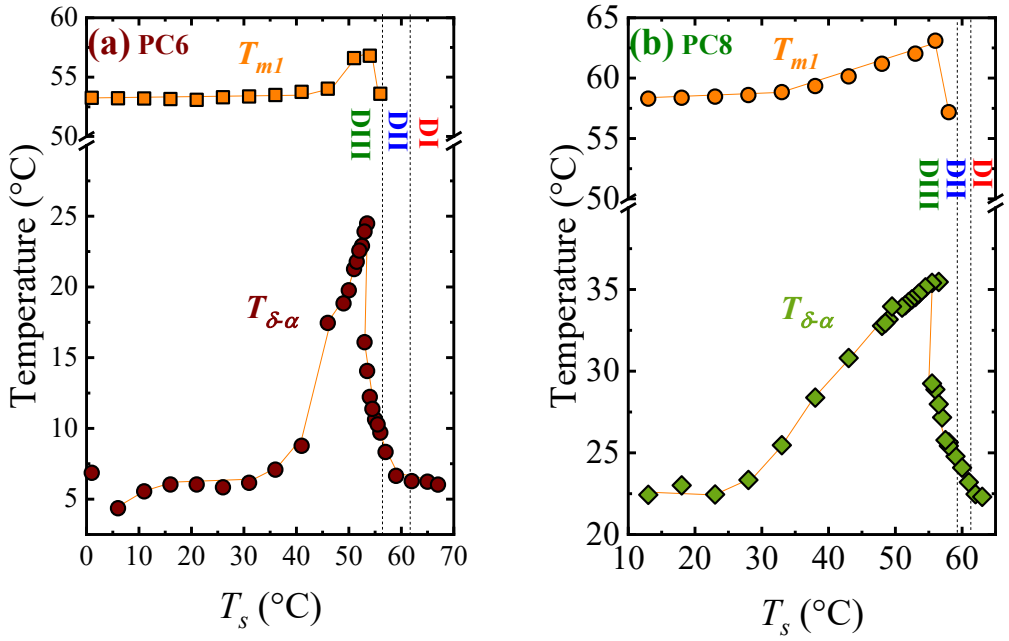

Figure 4. Variation of the endothermic δ to α transition, $T_{\delta-\alpha}$, and the highest melting point, T_{m1}, as a function of T_s, for (a) PC6, and (b) PC8. The $T_{\delta-\alpha}$ and T_{m1} values were obtained from SN experiments at selected T_s, including those used in SSA experiments. The vertical dashed line separates *Domains I, II,* and *III*. For clarity, the plotted T_{m1} data corresponds to selected T_s values.

Figure 4 shows that higher T_s values (where annealing of thicker crystals occurs) produce the more significant changes in the δ to α transition. For both PC6 and PC8, the endothermic peak of the δ to α transition, $T_{\delta-\alpha}$ starts to experience a significant shift at T_s = 53.5 °C (PC6) and 56.5 °C (PC8), the temperatures at which the annealing peak becomes more important. Afterward, the $T_{\delta-\alpha}$ reaches a maximum and progressively decreases, as thinner lamellae are annealed, until reaching a minimum point, at T_s ~ 31 °C (PC6), and T_s ~ 23 °C (PC8), which is similar to the $T_{\delta-\alpha}$ recorded in *Domain I*. Thus, the annealing of the thinnest lamellae at low T_s

values does not influence the $T_{\delta-\alpha}$. Figure 4 also includes the evolution of the highest annealing peak, T_{m1}, as a function of T_s. When *Domain III* starts, T_{m1} increases, reaching a maximum. In this region, it can be noticed that the annealing on the thicker crystals produces the most significant changes in the $T_{\delta-\alpha}$, corroborating that this transition depends on the stability of the crystals. After the maximum in T_{m1}, there is a progressive decrease as T_s decreases, similar to the one exhibited in the T_{m1} vs. T_s plot from SSA experiments (see Figure S5). At the lowest T_s values, the changes in T_{m1} are smaller or inexistent; hence the solid-solid transition is not significantly affected. To understand the structural and conformational changes involve in the solid-solid transitions, WAXS and FT-IR analyses were performed and the results are shown below.

3.3. *In-situ* WAXS/SSA experiments

For the structural characterization, we have selected the SSA protocol conditions. The SSA protocol was carried out *in-situ,* and simultaneously WAXS patterns were taken. We focused on the WAXS analysis during the final heating after the SSA protocol was applied to the samples. Figures 5 and 6 show WAXS patterns taken during the final heating performed to SSA-fractionated PC6 and PC8, respectively, and the evolution of the main planes *d*-spacing as a function of the temperature.

Both PC6 and PC8 crystallize in a monoclinic unit cell. The crystalline structure of PC6 has not been solved on basis of X-ray fiber patterns. The low molecular weight poly (hexamethylene carbonate)-glycols have been studied by a combination of 1D WAXS and conformation simulation.[43] It shows the following dimensions: a = 0.746 nm, b = 0.631 nm, c = 2.25 nm and α = 60° (considering the a-axis as the unique axis), and its WAXS pattern exhibited two main

reflections at q=14.3 nm^{-1} (2θ = 20.1°) and 16.8 nm^{-1} (2θ = 23.8°) (i.e., d-spacing of 0.441 and 0.373 nm, respectively), corresponding to the *(110)* and *(200)* planes, respectively.

As we already mentioned, PC8 possesses an α or β phase depending on the temperature. Both monoclinic structures were characterized by Zhao et al.[29] For the α phase, the unit cell parameters are a = 0.77 nm, b = 1.01 nm, c (fiber axis) = 2.52 nm, and α = 31.5°, and their main peaks at q = 14.5 nm^{-1} (2θ = 20.45°) and 16.4 nm^{-1} (2θ = 23.14°) (i.e., d-spacing of 0.430 and 0.380 nm, respectively) indexed to the *(110)* and *(200)* planes. For the β phase or Brill-like phase, the main reflections merged to a single one, at q = 15.5 nm^{-1} (2θ = 21.91°) with the characteristic d-spacing = 0.41 nm, which can be indexed to the *(110)/(200)* planes. In this case, the unit cell dimensions are a = 0.81 nm, b = 0.89 nm, c (chain axis) = 2.42 nm, and α = 31.9°.[29] In both cases, the unit cell parameters have been estimated by taking the a-axis as a unique axis and selecting monoclinic angles lower than 90°.

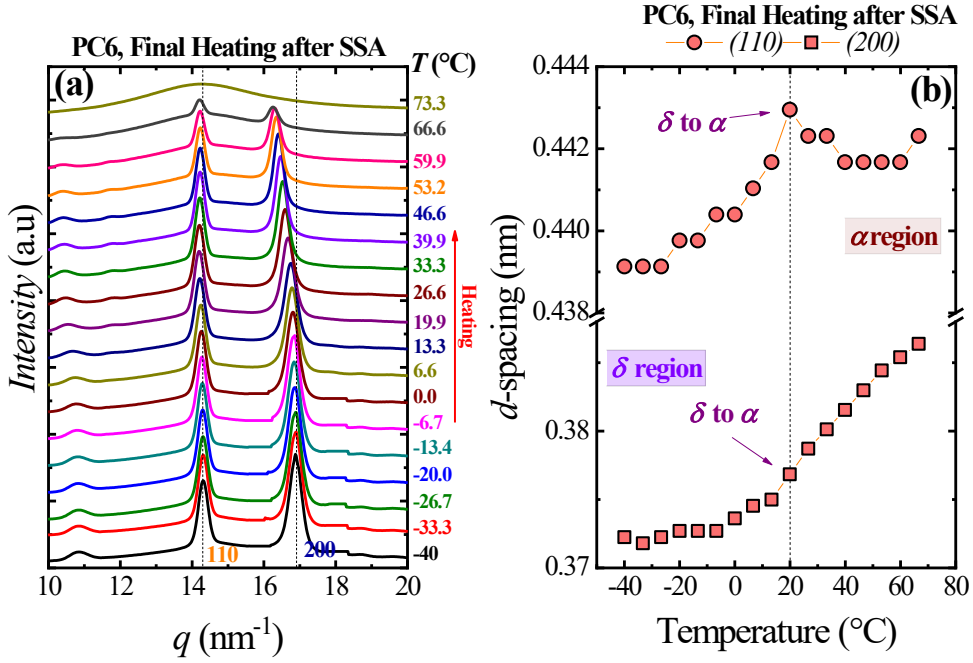

Figure 5. (a) WAXS patterns of PC6 taken during the final heating after SSA, and (b) *d*-spacing for the indicated (with vertical dashed lines) *(110)* and *(200)* planes (see Figure 5a), as a function of the temperature. The arrows in Figure 5b indicate the δ to α transition. The vertical dashed line indicated the detected (by DSC) δ to α transition.

As we show in the final SSA heating scan by DSC, the phase at low temperatures corresponds to the δ phase and the one at high temperatures to the α phase. Figure 5a shows the WAXS patterns taken during the SSA final heating. It is observed that the main reflections are shifted to higher q values (hence higher *d*-spacing) as the temperature increases, especially at ~ 20 °C, corroborating the SSA results (see Figure 2). The evolution of the *d*-spacing for the main planes, d_{110} and d_{200}, as a function of the temperature (see Figure 5b), clarifies the temperature position of the δ to α transition. The δ phase is characterized by lower *d*-spacing and lower unit cell dimensions than the α phase.

Figure 5b shows that the *d*-spacing remains almost constant at low temperatures (< 20 °C), indicating the presence of the δ phase. As the temperature increases, the *d*-spacing increases, especially the d_{200}, starting at ~ 7 °C, which is the onset of the δ to α transition temperature detected by SSA (Figure 2). At ~ 20 °C, which corresponds to the δ to α transition peak, detected also by SSA (see the vertical dashed line in Figure 5b), there is a higher increase of the d_{200} and d_{110}. The d_{110} exhibits a maximum. As the temperature increases, the α phase melts at ~ 60 °C, as in the SSA results. The melt of the α phase is reflected in a rise in the *d*-spacing resulting from the thermal expansion.

During the final heating after applying the SSA protocol to PC8, two solid-solid transitions are observed. The WAXS patterns and *d*-spacing as a function of the temperature are shown in Figures 6a and b.

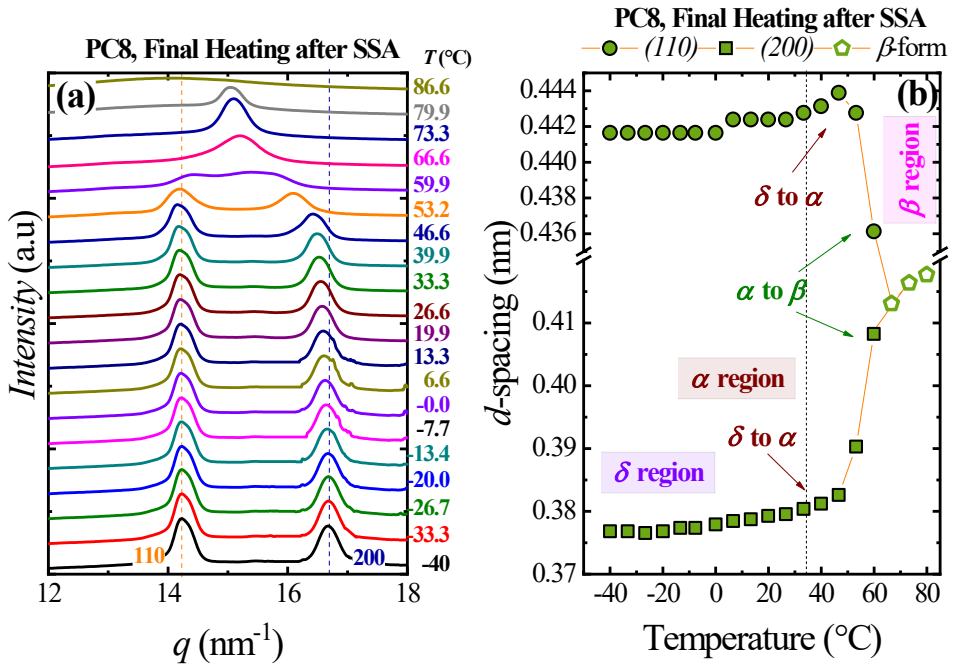

Figure 6. (a) WAXS patterns of PC8 taken during the final heating after SSA, and (b) *d*-spacing for the indicated (with vertical dashed lines) *(110)* and *(200)* planes (see Figure 6a), as a function of the temperature. The arrows in Figure 6b indicate the δ to α and α to β transitions. The vertical dashed line indicated the detected (by DSC) δ to α transition.

Figures 6a and b show that at low temperatures (− 40 to 0 °C), the position of the peaks remains practically unchanged, and it is only at $T > 0$ °C that a slight increase of the d_{200} is recorded. Thus, at low temperatures, the δ phase is present, and it is characterized by low *d*-spacing, exhibiting the lowest unit cell dimensions. At ~ 40 °C, the increase of the d_{110} and d_{200} is more pronounced due to the δ to α transition. Such change is reflected in a significant endothermic peak in the final SSA DSC heating scan (see Figure 2). At T > 40 °C, PC8 is already in the α phase. This phase is quickly transformed to the β phase at ~ 60 °C. The transformation towards the β phase is reflected in the combined d_{200} increase and d_{110} decrease

(see 50 to 60 °C range), merging in a single $d_{110/200}$, corresponding to the β phase, which melts at $T > 60$ °C.

Both PC6 and PC8 exhibit the lowest dimensions (i.e., lowest *d*-spacing) in the δ phase, compared to the α (PC6) or α and β ones (PC8), in line with our preceding work.[31] Such reduced dimensions suggest a more efficient chain packing in the δ phase crystals. Thus, upon heating, after the SSA treatment, the material experiences a transition from a tight package, in the δ phase, to an enlarged one in the α phase. Interestingly, the d_{100} and $d_{010/110}$ evolution with temperature shown in different polyamides (e.g., PA26, PA46, and PA66[17]) before the Brill transition resembles the *d*-spacing evolution found in this work. In fact, the PDC-6 (same n_{CH2} as the PC6), which has stronger dipolar interactions, presents a Brill transition process,[30,42] similar to the polyamides.[17]

3.4. Simultaneous FT-IR/SSA experiments

We studied FT-IR spectra during *in-situ* SSA experiments, following the final heating after SSA fractionating. Different spectral regions have been studied, detecting the strong bands related to carbonyl and methylene vibrations described in our previous work,[32] and recently reported bands associated with the δ to α transition (e.g., ordered and disordered methylene conformations).[31]

The solid-solid transition-related bands shown below have only been reported in our previous work,[31] and understanding their origin is beyond the scope of the present work. However, as we determined in our previous work,[31] the δ to α transition is related to a transition between disordered methylene groups (α phase) to ordered ones (δ phase). New absorption bands characterize the ordered conformations. Figure 7 shows selected absorption regions; for PC6, we

focus on the regions from 1500 to 1300 cm^{-1} (Figure 7a) and 1160 to 980 cm^{-1} (Figure 7b), and for PC8 on the regions from 1500 to 1300 cm^{-1} (Figure 7c) and 1000 to 900 cm^{-1} (Figure 7d).

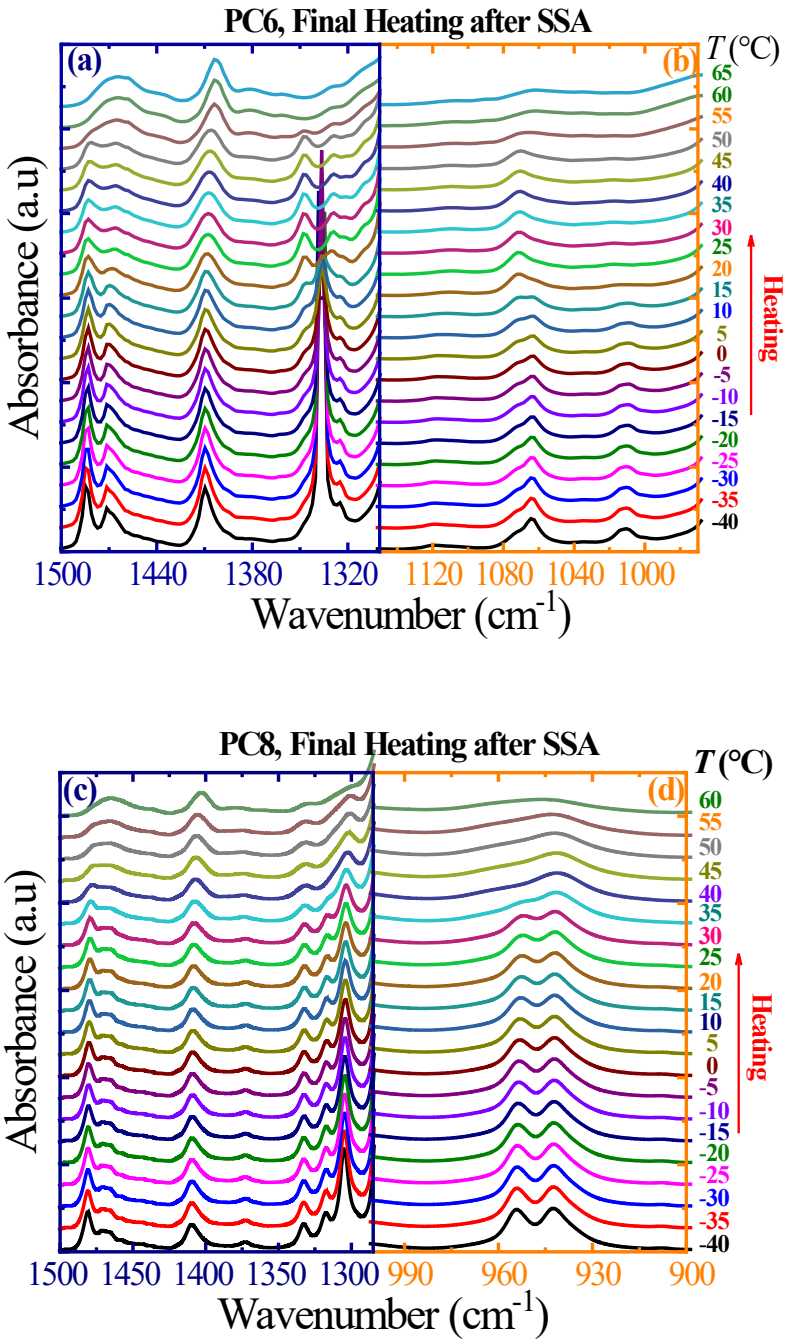

Figure 7. FT-IR spectra recorded during the final heating after SSA for PC6 in the range of (a) 1500 to 1300 cm^{-1}, and (b) 1160 to 980 cm^{-1}; and for PC8 in the range of (c) 1500 to 1285 cm^{-1} and (d) 1000 to 900 cm^{-1}.

We studied the evolution of the *gauche* (1460 cm^{-1}), and *trans* (1482 cm^{-1}) conformation bands in both PC6 (Figure 7a) and PC8 (Figure 7c), as in previous works.[29, 31, 32] Figures 7a and c, clearly show that the band at 1482 cm^{-1} is stronger at low temperatures (δ phase) and its intensity decreases upon heating (α phase), being comparable with the band at 1460 cm^{-1}. Thus, this behavior evidences that the relative intensity (I_{1482}/I_{1460}) depends on the temperature, indicating a strong dominance of the *trans* conformation (i.e., $I_{1482}/I_{1460} >> 1.0$) in the δ phase, and a decrease of such dominance (i.e., $I_{1482}/I_{1460} > 1.0$) in the α phase (see Figure S8). In the case of the PC8, the *trans/gauche* coexistence (see Figure 7c) conformation at high temperatures is characteristic of the β phase[29, 31] (see Figure S8b). The δ to α and α to β transitions are observed at the same range of temperatures reported in the SSA test (see Figure 2).

Figure 8 shows variation in absorbance as a function of the temperature, for selected absorption bands in 1350 to 1250 cm^{-1} region. The aim of Figure 8 is to illustrate that the characteristics bands of the δ phase disappear at the transition temperature, found by DSC, as a result of the disordered conformations. It is worth noting that other minor changes (e.g., changes in absorbance or shift in the main bands) might be related to the solid-solid transitions. Still, here, for clarity, we focus on the appearance or disappearance of absorption bands. The absorption bands related to other regions are plotted in Figures S9 and S10.

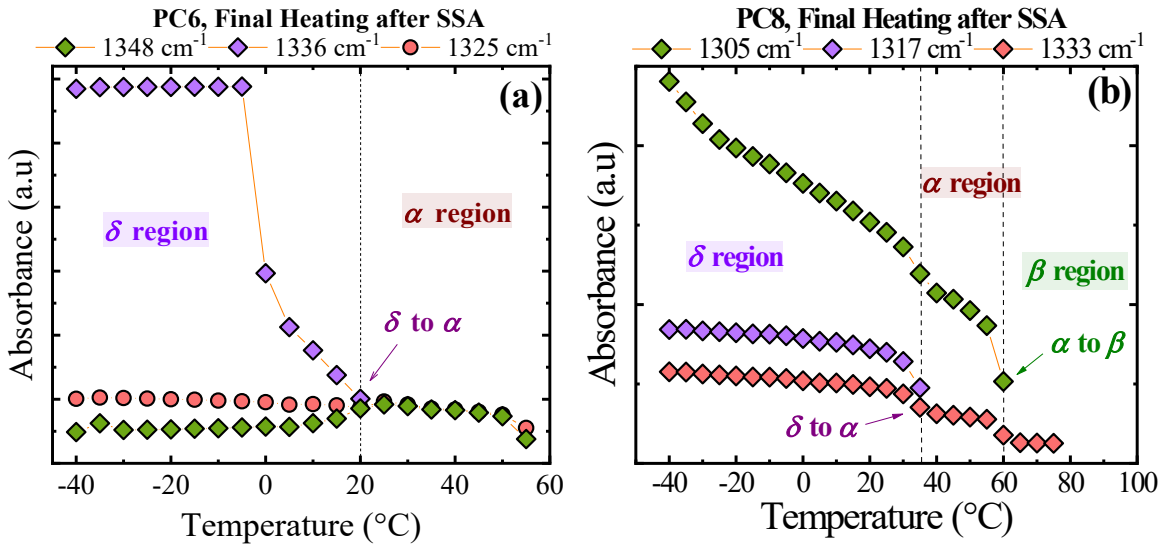

Figure 8. Variation of the absorbance, during the final heating after SSA, for (a) PC6 absorption bands at 1348, 1336, and 1325 cm^{-1}, and (b) PC8 absorption bands at 1305, 1317, and 1333 cm^{-1}, as a function of the temperature. The vertical dashed lines indicate the transition temperature which coincided with the one detected during the SSA experiments performed in the DSC.

Figures 7a and 8a show that at low temperatures (T < 20 °C) the bands at 1347, 1336, and 1328 cm^{-1} are present. Upon heating, the band at 1336 cm^{-1}, which is characteristic of the δ phase, disappears at ~ 20 °C, evidencing the δ to α transition, as illustrated in Figure 8a. Similarly, Figure 7b and S9 show that the characteristic bands of the δ phase at ~ 1011 cm^{-1} (Figure 6b) and at ~ 755 cm^{-1} (Figure S9c show the region related to the conformational disordering of methylene segments region[44-47]), disappears upon heating at ~ 20 °C (see Figure S9), indicating the δ to α transition. Thus, the bands at 1336, 1011 and 755 cm^{-1} are characteristic of the δ phase, and their disappearance indicates the solid-solid transition.

The behavior of the PC8 is similar during the final heating after SSA, as illustrated in Figure 8b. In this case, the characteristics bands of the δ phase are located at 1317 cm^{-1} and 955 cm^{-1} (see Figures 7c and d) disappearing during the heating at T > 30 °C (see Figures 8b and S10).

Figure 7c shows that the bands at 1332 and 1303 cm^{-1} become less sharp and intense upon heating, indicating a different crystalline phase, the α or β phase, while the band at 942 cm^{-1} is slightly shifted to 940 cm^{-1} around 45 °C. This shift can be attributed to the α to β transition. At $T > 45$ °C (β phase), the band at 940 cm^{-1} becomes weaker upon heating.

To sum up, the δ phase is characterized by more efficient chain packing in the crystals (see Section 3.3) due to the more ordered conformation of the methylene groups, by the extra absorption bands, and the *trans* conformation dominance of the chains. In contrast, the α phase, where chains are less efficiently packed in the crystals (see Section 3.3), exhibited more disordered conformations of the methylene groups, characterized by the absence of the δ bands, and less dominant *trans* conformation of the chains.

4. CONCLUSIONS

For the first time, the SSA technique was used to detect the denoted δ to α solid-solid transitions for PC6 and PC8, demonstrating a helpful approach. During the final heating after SSA fractionation, the endothermic peak of the δ to α transition shows higher temperatures and enthalpies as compared to the endotherm found during a standard second heating DSC scan. Moreover, the δ to α peak remains unfractionated. Self-nucleation and SSA tests with different experimental conditions revealed that the solid-solid transition DSC signals are particularly improved when the thickest lamellae of α and β crystals are annealed (i.e., different levels of crystal stability are reached) in *Domain III.* In contrast, *Domains I* and *II* do not affect the solid-solid transitions since they do not produce crystal stability changes. *In-situ* SSA experiments were performed by WAXS and FT-IR. They reveal that the δ to α solid-solid transition corresponds to a transformation of ordered (δ phase) to disordered (α phase) methylene

conformations, thus enabling a more efficient (δ phase) to less efficient (α phase) chain packing in the crystals.

ACKNOWLEDGMENTS

We would like to thank the financial support provided by the National Key R&D Program of China (2017YFE0117800), the National Natural Science Foundation of China (51820105005, 21922308, and 52050410327). We also acknowledge the financial support from the BIODEST project; this project has received funding from the European Union's Horizon 2020 research and innovation program under the Marie Skłodowska-Curie Grant Agreement No. 778092. This work has also received funding from MINECO through project MAT2017-83014-C2-1-P and from Basque Government through grant IT1309-19. R.A.P.-C is supported by the China Postdoctoral Science Foundation (2020M670462). G.L. is grateful to the Youth Innovation Promotion Association of the Chinese Academy of Sciences (Y201908). We also thank the BSRF (beamline 1W2A) for providing the beamtime.

Supporting Information

Non-isothermal DSC cooling and heating scans, extra SN and SSA results at varied conditions, and extra FT-IR analysis curves at the final heating after SSA fractionation.

5. REFERENCES

1. Müller, A. J.; Michell, R. M.; Pérez, R. A.; Lorenzo, A. T. Successive Self-nucleation and Annealing (SSA): Correct design of thermal protocol and applications. *European Polymer Journal* **2015,** 65, 132-154 DOI: https://doi.org/10.1016/j.eurpolymj.2015.01.015.
2. Müller, A. J.; Hernández, Z. H.; Arnal, M. L.; Sánchez, J. J. Successive self-nucleation/annealing (SSA): A novel technique to study molecular segregation during crystallization. *Polymer Bulletin* **1997,** 39 (4), 465-472 DOI: 10.1007/s002890050174.

3. Müller, A. J.; Arnal, M. L. Thermal fractionation of polymers. *Progress in Polymer Science* **2005,** 30 (5), 559-603 DOI: https://doi.org/10.1016/j.progpolymsci.2005.03.001.
4. Lorenzo, A. T.; Arnal, M. L.; Müller, A. J.; Boschetti de Fierro, A.; Abetz, V. High Speed SSA Thermal Fractionation and Limitations to the Determination of Lamellar Sizes and Their Distributions. *Macromolecular Chemistry and Physics* **2006,** 207 (1), 39-49 DOI: 10.1002/macp.200500437.
5. Müller, A. J.; Lorenzo, A. T.; Arnal, M. L. Recent Advances and Applications of "Successive Self-Nucleation and Annealing" (SSA) High Speed Thermal Fractionation. *Macromolecular Symposia* **2009,** 277 (1), 207-214 DOI: 10.1002/masy.200950325.
6. Lorenzo, A. T.; Arnal, M. L.; Müller, A. J.; Lin, M.-C.; Chen, H.-L. SAXS/DSC Analysis of the Lamellar Thickness Distribution on a SSA Thermally Fractionated Model Polyethylene. *Macromolecular Chemistry and Physics* **2011,** 212 (18), 2009-2016 DOI: 10.1002/macp.201100240.
7. Arnal, M. L.; Sánchez, J. J.; Müller, A. J. Miscibility of linear and branched polyethylene blends by thermal fractionation: use of the successive self-nucleation and annealing (SSA) technique. *Polymer* **2001,** 42 (16), 6877-6890 DOI: https://doi.org/10.1016/S0032-3861(01)00177-X.
8. Lorenzo, A. T.; Arnal, M. L.; Müller, A. J.; Boschetti de Fierro, A.; Abetz, V. Confinement effects on the crystallization and SSA thermal fractionation of the PE block within PE-b-PS diblock copolymers. *European Polymer Journal* **2006,** 42 (3), 516-533 DOI: https://doi.org/10.1016/j.eurpolymj.2005.09.001.
9. Sangroniz, L.; Wang, B.; Su, Y.; Liu, G.; Cavallo, D.; Wang, D.; Müller, A. J. Fractionated crystallization in semicrystalline polymers. *Progress in Polymer Science* **2021,** 115, 101376 DOI: https://doi.org/10.1016/j.progpolymsci.2021.101376.
10. Colonna, S.; Pérez-Camargo, R. A.; Chen, H.; Liu, G.; Wang, D.; Müller, A. J.; Saracco, G.; Fina, A. Supernucleation and Orientation of Poly(butylene terephthalate) Crystals in Nanocomposites Containing Highly Reduced Graphene Oxide. *Macromolecules* **2017,** 50 (23), 9380-9393 DOI: 10.1021/acs.macromol.7b01865.
11. Pérez-Camargo, R. A.; Liu, G.; Cavallo, D.; Wang, D.; Müller, A. J. Effect of the Crystallization Conditions on the Exclusion/Inclusion Balance in Biodegradable Poly(butylene succinate-ran-butylene adipate) Copolymers. *Biomacromolecules* **2020,** 21 (8), 3420-3435 DOI: 10.1021/acs.biomac.0c00847.
12. Arandia, I.; Mugica, A.; Zubitur, M.; Iturrospe, A.; Arbe, A.; Liu, G.; Wang, D.; Mincheva, R.; Dubois, P.; Müller, A. J. Application of SSA thermal fractionation and X-ray diffraction to elucidate comonomer inclusion or exclusion from the crystalline phases in poly(butylene succinate-ran-butylene azelate) random copolymers. *Journal of Polymer Science Part B: Polymer Physics* **2016,** 54 (22), 2346-2358 DOI: 10.1002/polb.24146.
13. Pérez-Camargo, R. A.; d'Arcy, R.; Iturrospe, A.; Arbe, A.; Tirelli, N.; Müller, A. J. Influence of Chain Primary Structure and Topology (Branching) on Crystallization and Thermal Properties: The Case of Polysulfides. *Macromolecules* **2019,** 52 (5), 2093-2104 DOI: 10.1021/acs.macromol.8b02659.
14. Pérez, R. A.; Córdova, M. E.; López, J. V.; Hoskins, J. N.; Zhang, B.; Grayson, S. M.; Müller, A. J. Nucleation, crystallization, self-nucleation and thermal fractionation of cyclic and linear poly(ε-caprolactone)s. *Reactive and Functional Polymers* **2014,** 80, 71-82 DOI: https://doi.org/10.1016/j.reactfunctpolym.2013.10.013.

15. Li, X.; Wang, L.; Wang, D.; Müller, A. J.; Dong, X. Competition between Chain Extension and Crosslinking in Polyamide 1012 during High-Temperature Thermal Treatments as Revealed by Successive Self-Nucleation and Annealing Fractionation. *Macromolecules* **2021**, 54 (16),7552-7563 DOI: 10.1021/acs.macromol.1c01252.
16. Lotz, B. A Fresh Look at the Structures of Nylons and the Brill Transition. *Adv. Fiber Mater* **2021**, 3, 203-209 DOI: 10.1007/s42765-021-00085-9.
17. Lotz, B. Brill Transition in Nylons: The Structural Scenario(). *Macromolecules* **2021**, 54 (2), 565-583 DOI: 10.1021/acs.macromol.0c02409.
18. Feldman, A. Y.; Wachtel, E.; Vaughan, G. B. M.; Weinberg, A.; Marom, G. The Brill Transition in Transcrystalline Nylon-66. *Macromolecules* **2006,** 39 (13), 4455-4459 DOI: 10.1021/ma060487h.
19. Ramesh, C.; Keller, A.; Eltink, S. J. E. A. Studies on the crystallization and melting of nylon-6,6: 1. The dependence of the Brill transition on the crystallization temperature. *Polymer* **1994,** 35 (12), 2483-2487 DOI: https://doi.org/10.1016/0032-3861(94)90367-0.
20. Starkweather Jr., H. W.; Whitney, J. F.; Johnson, D. R. Crystalline order in nylon 66. **1963,** 1 (2), 715-723 DOI: https://doi.org/10.1002/pol.1963.100010211.
21. Jones, N. A.; Atkins, E. D. T.; Hill, M. J.; Cooper, S. J.; Franco, L. Chain-folded lamellar crystals of aliphatic polyamides. Investigation of nylons 4 8, 4 10, 4 12, 6 10, 6 12, 6 18 and 8 12. *Polymer* **1997,** 38 (11), 2689-2699 DOI: https://doi.org/10.1016/S0032-3861(97)85603-0.
22. Jones, N. A.; Atkins, E. D. T.; Hill, M. J. Comparison of Structures and Behavior on Heating of Solution-Grown, Chain-Folded Lamellar Crystals of 31 Even−Even Nylons. *Macromolecules* **2000,** 33 (7), 2642-2650 DOI: 10.1021/ma9919559.
23. Li, Y.; Yan, D.; Zhu, X. Crystalline transition in Nylon 10 10. *Macromolecular Rapid Communications* **2000,** 21 (18), 1282-1285 DOI: https://doi.org/10.1002/1521-3927(20001201)21:18<1282::AID-MARC1282>3.0.CO;2-X.
24. Yan, D.; Li, Y.; Zhu, X. Brill transition in Nylon 10 12 investigated by variable temperature XRD and real time FT-IR. *Macromolecular Rapid Communications* **2000,** 21 (15), 1040-1043 DOI: https://doi.org/10.1002/1521-3927(20001001)21:15<1040::AID-MARC1040>3.0.CO;2-X.
25. Yang, X.; Tan, S.; Li, G.; Zhou, E. Dependence of the Brill Transition on the Crystal Size of Nylon 10 10. *Macromolecules* **2001,** 34 (17), 5936-5942 DOI: 10.1021/ma002091q.
26. Wang, Y.; Zhu, P.; Qian, C.; Zhao, Y.; Wang, L.; Wang, D.; Dong, X. The Brill Transition in Long-Chain Aliphatic Polyamide 1012: The Role of Hydrogen-Bonding Organization. *Macromolecules* **2021**, 54 (14), 6835-6844 DOI: 10.1021/acs.macromol.1c01141.
27. Lotz, B. Original Crystal Structures of Even–Even Polyamides Made of Pleated and Rippled Sheets. *Macromolecules* **2021,** 54 (2), 551-564 DOI: 10.1021/acs.macromol.0c02404.
28. Puiggalí, J. Aliphatic polyamides (nylons): Interplay between hydrogen bonds and crystalline structures, polymorphic transitions and crystallization. *Polymer Crystallization* **2021**, 4 (4), e10199 DOI: https://doi.org/10.1002/pcr2.10199.
29. Zhao, T.-P.; Ren, X.-K.; Zhu, W.-X.; Liang, Y.-R.; Li, C.-C.; Men, Y.-F.; Liu, C.-Y.; Chen, E.-Q. "Brill Transition" Shown by Green Material Poly(octamethylene carbonate). *ACS Macro Letters* **2015,** 4 (3), 317-321 DOI: 10.1021/acsmacrolett.5b00045.
30. Zhao, T.-P.; Celli, A.; Ren, X.-K.; Xu, J.-R.; Yang, S.; Liu, C.-Y.; Chen, E.-Q. Sharp and strong "Brill transition" of poly(hexamethylene dithiocarbonate). *Polymer* **2017,** 113, 267-273 DOI: https://doi.org/10.1016/j.polymer.2017.02.045.

31. Pérez-Camargo, R. A.; Liu, G.; Meabe, L.; Zhao, Y.; Sardon, H.; Wang, D.; Müller, A. J. Solid–Solid Crystal Transitions (δ to α) in Poly(hexamethylene carbonate) and Poly(octamethylene carbonate). *Macromolecules* **2021**, 54(15), 7258-7268 DOI: 10.1021/acs.macromol.1c01188.
32. Pérez-Camargo, R. A.; Meabe, L.; Liu, G.; Sardon, H.; Zhao, Y.; Wang, D.; Müller, A. J. Even–Odd Effect in Aliphatic Polycarbonates with Different Chain Lengths: from Poly (Hexamethylene Carbonate) to Poly (Dodecamethylene Carbonate). *Macromolecules* **2020,** 54 (1), 259-271 DOI: 10.1021/acs.macromol.0c02374.
33. Meabe, L.; Lago, N.; Rubatat, L.; Li, C.; Müller, A. J.; Sardon, H.; Armand, M.; Mecerreyes, D. Polycondensation as a Versatile Synthetic Route to Aliphatic Polycarbonates for Solid Polymer Electrolytes. *Electrochimica Acta* **2017,** 237, 259-266 DOI: https://doi.org/10.1016/j.electacta.2017.03.217.
34. Sun, J.; Kuckling, D. Synthesis of high-molecular-weight aliphatic polycarbonates by organo-catalysis. *Polymer Chemistry* **2016,** 7 (8), 1642-1649 DOI: 10.1039/c5py01843a.
35. Fillon, B.; Wittmann, J. C.; Lotz, B.; Thierry, A. Self‐nucleation and recrystallization of isotactic polypropylene (α phase) investigated by differential scanning calorimetry. *Journal of Polymer Science Part B: Polymer Physics* **1993,** 31 (10), 1383-1393 DOI: 10.1002/polb.1993.090311013.
36. Michell, R. M.; Mugica, A.; Zubitur, M.; Müller, A. J., Self-Nucleation of Crystalline Phases Within Homopolymers, Polymer Blends, Copolymers, and Nanocomposites. In *Polymer Crystallization I: From Chain Microstructure to Processing*, Auriemma, F., Alfonso, G. C., de Rosa, C., Eds. Springer International Publishing: Cham, 2017; pp 215-256.
37. Sangroniz, L.; Alamo, R. G.; Cavallo, D.; Santamaría, A.; Müller, A. J.; Alegría, A. Differences between Isotropic and Self-Nucleated PCL Melts Detected by Dielectric Experiments. *Macromolecules* **2018,** 51 (10), 3663-3671 DOI: 10.1021/acs.macromol.8b00708.
38. Sangroniz, L.; Cavallo, D.; Müller, A. J. Self-Nucleation Effects on Polymer Crystallization. *Macromolecules* **2020,** 53 (12), 4581-4604 DOI: 10.1021/acs.macromol.0c00223.
39. Wang, M.; Li, J.; Shi, G.; Liu, G.; Müller, A. J.; Wang, D. Suppression of the Self-Nucleation Effect of Semicrystalline Polymers by Confinement. *Macromolecules* **2021,** 54 (8), 3810-3821 DOI: 10.1021/acs.macromol.1c00485.
40. Lorenzo, A. T.; Arnal, M. L.; Sánchez, J. J.; Müller, A. J. Effect of annealing time on the self-nucleation behavior of semicrystalline polymers. *Journal of Polymer Science Part B: Polymer Physics* **2006,** 44 (12), 1738-1750 DOI: 10.1002/polb.20832.
41. Sangroniz, L.; Sangroniz, A.; Meabe, L.; Basterretxea, A.; Sardon, H.; Cavallo, D.; Müller, A. J. Chemical Structure Drives Memory Effects in the Crystallization of Homopolymers. *Macromolecules* **2020,** 53 (12), 4874-4881 DOI: 10.1021/acs.macromol.0c00751.
42. Berti, C.; Celli, A.; Marchese, P.; Marianucci, E.; Marega, C.; Causin, V.; Marigo, A. Aliphatic poly(alkylene dithiocarbonate)s: Thermal properties and structural characteristics of poly(hexamethylene dithiocarbonate). *Polymer* **2007,** 48 (1), 174-182 DOI: https://doi.org/10.1016/j.polymer.2006.11.035.
43. Masubuchi, T.; Sakai, M.; Kojio, K.; Furukawa, M.; Aoyagi, T. Structure and Properties of Aliphatic Poly(carbonate) glycols with Different Methylene Unit Length. *e-Journal of Soft Materials* **2007,** 3, 55-63 DOI: 10.2324/ejsm.3.55.
44. Yoshioka, Y.; Tashiro, K.; Ramesh, C. Structural change in the Brill transition of Nylon m/n (2) conformational disordering as viewed from the temperature-dependent infrared spectral

measurements. *Polymer* **2003,** 44 (20), 6407-6417 DOI: https://doi.org/10.1016/S0032-3861(03)00593-7.
45. Snyder, R. G.; Schachtschneider, J. H. Vibrational analysis of the n-paraffins—I: Assignments of infrared bands in the spectra of C3H8 through n-C19H40. *Spectrochimica Acta* **1963,** 19 (1), 85-116 DOI: https://doi.org/10.1016/0371-1951(63)80095-8.
46. Schachtschneider, J. H.; Snyder, R. G. Vibrational analysis of the n-paraffins—II: Normal co-ordinate calculations. *Spectrochimica Acta* **1963,** 19 (1), 117-168 DOI: https://doi.org/10.1016/0371-1951(63)80096-X.
47. Kobayashi, S.; Tadokoro, H.; Chatani, Y. Structural studies on polyethers, [–(CH2)m–O–]n. VI. The higher members with m = 6–10, 12. *Die Makromolekulare Chemie* **1968,** 112 (1), 225-241 DOI: 10.1002/macp.1968.021120120.